Integrin β_1-focal adhesion kinase signaling directs the proliferation of metastatic cancer cells disseminated in the lungs

Tsukasa Shibue[a,b] and Robert A. Weinberg[a,b,c,1]

[a]Whitehead Institute for Biomedical Research, 9 Cambridge Center, Cambridge, MA 02142; and [b]Ludwig Center for Molecular Oncology, and [c]Department of Biology, Massachusetts Institute of Technology, 77 Massachusetts Ave., Cambridge, MA 02139

Contributed by Robert A. Weinberg, April 23, 2009 (sent for review March 3, 2009)

The development of metastases is an extended and inefficient process involving multiple steps. The last of these involves the growth of micrometastases into macroscopic tumors. We show here that intravenously injected, nonmetastatic cancer cells cease proliferating after extravasating into the parenchyma of the lungs; this response is attributable to the cells inability to trigger adhesion-related signaling events when they are scattered sparsely within the extracellular matrix (ECM) of the parenchyma. We recapitulate this situation by culturing these nonmetastatic cells at low seeding density in ECM-derived gels in vitro, in which they undergo cell-cycle arrest resulting, in part, from insufficient activation of focal adhesion kinase (FAK). Metastatic cancer cells, in contrast, show sufficient FAK activation to enable their proliferation within ECM gels in vitro and continue cell-cycle progression within the lung parenchyma in vivo. Activation of FAK in these metastatic cells depends on expression of the β_1 subunit of integrins, and proliferation of these cells after extravasation in the lungs is diminished by knocking down the expression of either FAK or integrin β_1. These results demonstrate the critical role of integrin β_1-FAK signaling axis in controlling the initial proliferation of micrometastatic cancer cells disseminated in the lungs.

dormancy | micrometastasis | cell-matrix adhesion

Cancer cells pass through a sequence of multiple steps to generate macroscopic metastases. These include invasion of host tissues adjacent to the primary tumor, entrance into the systemic vasculature, dissemination via the circulation, arrest in microvasculature, extravasation into the parenchyma of distant organs, and proliferation at these ectopic sites to form secondary colonies; the last of these steps, involving the growth of micrometastases into macroscopic tumors, is often termed "colonization" (1). This last step is likely to be the least efficient step in the invasion–metastasis cascade. For example, 30% of breast cancer patients are found to have hundreds, likely thousands of micrometastases in their bone marrow, but only half of these micrometastasis-positive patients will ever develop metastatic relapse (2). These relapses often become apparent 5, 10, or even 20 years after removal of the primary tumor and testify to the presence of disseminated, latent cancer cells that require many years to succeed in developing into macroscopic growths (3). Indeed, similar delayed-onset metastatic relapses are seen in multiple types of cancers, including renal cell carcinoma, melanoma, and osteosarcoma (4). These phenomena highlight the need to elucidate the mechanisms that enable metastasized cancer cells to colonize sites of dissemination.

Most disseminated cancer cells are rapidly eliminated by apoptosis in response to stresses associated with their transport or their inability to adapt to foreign tissue microenvironments (5). The survival of cells that have begun to proliferate in distant organ sites is also threatened, possibly by limited angiogenesis or by immune surveillance (5). These responses contrast with the observed behavior of many disseminated micrometastatic cancer cells that survive for prolonged periods of time in a dormant state, exhibiting neither proliferation nor apoptosis. Such cells were initially described experimentally in a mouse model (6), and evidence is accumulating for the presence of cells with similar properties in patients lacking any overt signs of metastasis (2, 7). The factors preventing the proliferation of these cancer cells and the resulting growth of micrometastases remain poorly understood.

In the present study, we have used a series of mouse mammary carcinoma cell lines composed of cells with differing abilities to proliferate after dissemination to distant organs including lungs and liver. These experiments have revealed a critical role of cell-matrix adhesions in governing this process, involving, notably, the integrin β_1-focal adhesion kinase (FAK) signaling axis.

Results

Behavior of D2 Mouse Mammary Carcinoma Cell Lines in an Experimental Model of Lung Metastasis. We used a set of mouse mammary carcinoma cells that consists of 3 distinct lines, D2.0R, D2.1, and D2A1, hereafter collectively referred to as "D2 cells" (8). Previous studies had shown comparable primary tumor incidence after implantation of these 3 cell populations in mouse mammary fat pads and the differing abilities of these primary tumors to subsequently form metastases in the lungs and liver (9). Thus, the D2.0R- and D2.1-derived tumors generated only rare metastases, whereas the D2A1-derived tumors spawned metastases efficiently. Moreover, D2.0R cells injected into the mesenteric vein successfully extravasated into the liver parenchyma but could not initiate proliferation in this site. In contrast, a substantial proportion of D2A1 cells began proliferating soon after extravasation into the liver parenchyma and eventually formed large numbers of macroscopic metastases (6).

We initially tested the behavior of the various D2 cells in an experimental model of lung metastasis. To enable direct comparisons of nonmetastatic and metastatic D2 cells, we labeled D2A1 cells with tdTomato, a variant of red fluorescent protein (RFP) (10), and coinjected these cells into the tail vein of BALB/c mice together with green fluorescent protein (GFP)-labeled D2.0R or D2.1 cells. As shown in Fig. 1*A*, multiple small clumps of cells were observed in the lungs at 2 days after injection, and the numbers and sizes of GFP-labeled D2.1 cell clumps and tdTomato-labeled D2A1 cell clumps were comparable at this time. However, as time went on, the clumps of D2A1 cells became larger, whereas those of D2.1 cells remained small, resulting in a substantial difference in the relative abundance of these cells in the lungs 24 days after injection (Fig. 1*A*). Similar differences in colony growth and relative abundance of cells in the lungs were observed when we coinjected GFP-labeled D2.0R cells and tdTomato-labeled D2A1 cells (data not shown, Fig. 1*A*).

Author contributions: T.S. designed research; T.S. performed research; T.S. and R.A.W. analyzed data; and T.S. and R.A.W. wrote the paper.

The authors declare no conflict of interest.

[1]To whom correspondence should be addressed. E-mail: weinberg@wi.mit.edu.

This article contains supporting information online at www.pnas.org/cgi/content/full/0904227106/DCSupplemental.

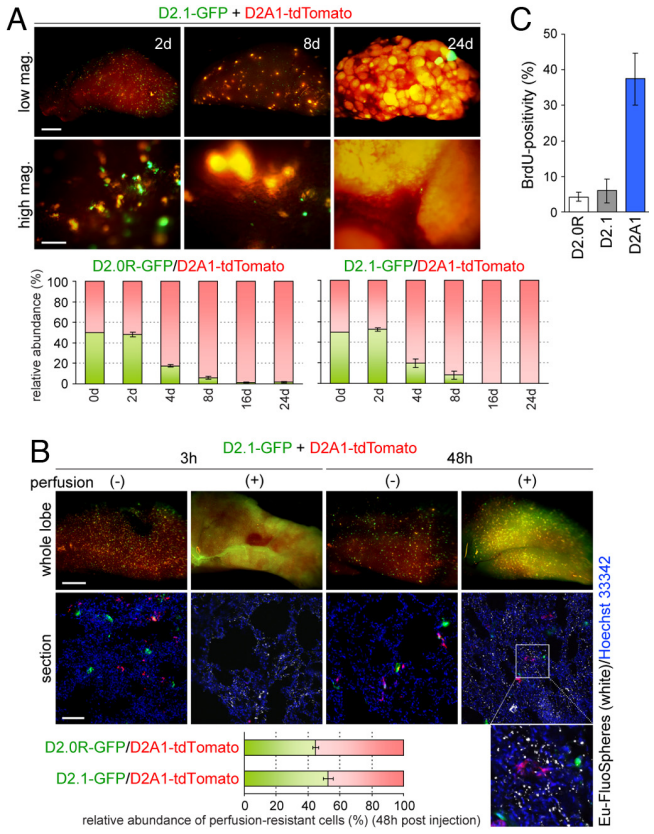

Fig. 1. Behavior of D2 cells in an experimental model of lung metastasis. (*A*) Equal numbers of GFP-labeled D2.0R or D2.1 cells (D2.0R-GFP and D2.1-GFP, respectively) and tdTomato-labeled D2A1 cells (D2A1-tdTomato) were coinjected into the tail vein, and the lungs were harvested at the indicated time points. Shown are the representative high (high mag.) and low magnification (low mag.) images of the left upper lobe of the lungs harboring D2.1-GFP and D2A1-tdTomato cells (*Top*). [Scale bar, 1 mm (low mag.); 0.1 mm (high mag.).] The relative abundance of GFP- and tdTomato-labeled cells in the lungs was analyzed by flow cytometry (FACS) (*Bottom Left*: D2.0R-GFP and D2A1-tdTomato; *Bottom Right*: D2.1-GFP and D2A1-tdTomato). (*B*) Lungs were harvested at the indicated time points after the coinjection of D2.1-GFP and D2A1-tdTomato cells, and frozen sections were prepared. Shown are the representative whole lobe (*Top* row) and section images (*Middle* row). An enlarged image of the boxed region within the rightmost section image is also presented (*Bottom Right*). In some of the mice, the lung vasculature was perfused by injecting PBS and FluoSpheres with europium luminescence (Eu-FluoSpheres) in the right ventricle just before harvesting the lungs. In the section images, fluorescent signals from Eu-FluoSpheres represent the lumina of microvessels (white), and the nuclei were stained with Hoechst 33422 (blue). [Scale bar, 1 mm (whole lobe); 0.2 mm (section).] Frozen sections of the lungs after the coinjection of D2.0R-GFP and D2A1-tdTomato cells were also prepared. The relative abundance of perfusion-resistant D2.0R-GFP and D2A1-tdTomato cells, and that of D2.1-GFP and D2A1-tdTomato cells, in the lungs at 48 h after injection were determined by direct counting on the sections (*Bottom*). (*C*) At 7 days after the injection of tdTomato-labeled D2 cells, the lung vasculature was perfused and the lungs were harvested. BrdU was i.p. injected twice, at 6 and 3 h before harvesting the lungs. The percentage of BrdU-positive cells within the tdTomato-expressing population was analyzed by BrdU staining and FACS. Values are means ± SEM ($n = 4$) (*A*–*C*).

We proceeded to measure the relative abilities of the various D2 cell populations to extravasate into the lung parenchyma. Accordingly, we injected the GFP- and tdTomato-labeled cells through the tail vein and, after various periods of time, perfused the lung microvasculature using fluorescence-labeled small polystyrene beads (FluoSpheres) that subsequently filled the capillary lumina (11). This procedure enabled us not only to trace the outlines of the microvasculature but also to flush out tumor cells that remained in the lumina of microvessels and thus had not yet extravasated. We found that the majority of fluorescence-labeled D2.1 and D2A1 cells that had remained in the lungs at 3 h after injection were cleared out by this perfusion procedure (Fig. 1*B*). At 48 h after injection, however, a substantial portion of these cell populations present in the lungs remained there after perfusion and, significantly, these perfusion-resistant populations contained comparable numbers of D2.1 and D2A1 cells (Fig. 1*B*). We also observed comparable numbers of perfusion-resistant D2.0R and D2A1 cells in the lungs after coinjecting these 2 different cell populations (Fig. 1*B*). Most of these perfusion-resistant cells were located at some distance from the FluoSphere-labeled vasculature (Fig. 1*B*), providing further indication that they had extravasated into the lung parenchyma.

These results suggested that the nonmetastatic D2.0R and D2.1 cells were as effective as the metastatic D2A1 cells in extravasating. We noted, however, that the extravasated D2.0R and D2.1 cells surviving in the lungs at 7 days after injection exhibited far less BrdU incorporation than corresponding D2A1 cells (Fig. 1*C*). Moreover, we observed comparable numbers of colonies of GFP-labeled D2.1 cells and those of tdTomato-labeled D2A1 cells in the lungs at 8 days after coinjecting equal numbers of these 2 different cell populations. This observation indicated that the persistence of D2.1-derived micrometastatic colonies in the lungs is comparable with that of D2A1-derived colonies, although the average size of D2A1-derived colonies was already far larger than that of D2.1-derived colonies at 8 days after injection (Fig. 1*A*). We also observed comparable numbers of GFP-labeled D2.0R cell colonies and tdTomato-labeled D2A1 cell colonies in the lungs at 8 days after coinjecting these 2 cell types (data not shown). These results collectively supported the notion that the inability of the D2.0R and D2.1 cells to eventually form macroscopic lung metastases was determined largely, if not entirely, by their inefficient proliferation after extravasation into the lung parenchyma.

Modeling the Differential Proliferation of D2 Cells in an In Vitro System. To uncover the cause(s) of the observed proliferation defect of the D2.0R and D2.1 cells, we attempted to recapitulate the postextravasation process with an in vitro experimental model. More specifically, we developed culture conditions that mimic certain aspects of the in vivo microenvironment surrounding recently extravasated cancer cells. It appears that most cancer cells, when introduced intravenously as single-cell suspensions, do not initially enjoy homotypic interactions with other cancer cells immediately after extravasation (12); instead, they are likely to be surrounded by stromal components of the parenchyma. Independent of this finding, others had shown that introducing cells into a 3-dimensional (3D) culture model, specifically in gels constructed of extracellular matrix (ECM) components, has profound effects on the behavior of such cells (13, 14). For these reasons, we embedded the 3 different D2 cell populations in several types of gels, each consisting of a distinct mixture of ECM components; these cells were prepared as single-cell suspensions and introduced into the gels at a low seeding density (500 cells/cm^2 bottom area) to ensure that they could not initially form extensive homotypic interactions with one another [supporting information (SI) Fig. S1*A*].

After 10 days of 3D culture, we observed 9.2- to 100-fold greater numbers of D2A1 cells compared with those of the other 2 lines, depending on the nature of the ECM gel used (Fig. S1). In contrast, when we plated these 3 cell populations under 2-dimensional (2D) conditions, i.e., on tissue culture plastic dishes without admixed ECM gels, the differences in the cell number after 10 days of culture were <3.5-fold (Fig. S1). This observation underscored the utility of the 3D culture model in studying the cause(s) underlying the differing rates of proliferation of the metastatic and nonmetastatic D2 cells after their extravasation into the lung parenchyma (Fig. 1*C*).

Among the 5 different types of ECM gels tested, Matrigel yielded the greatest difference in the resulting cell number between the D2A1 cells and the other 2 lines (Fig. S1), which encouraged us to

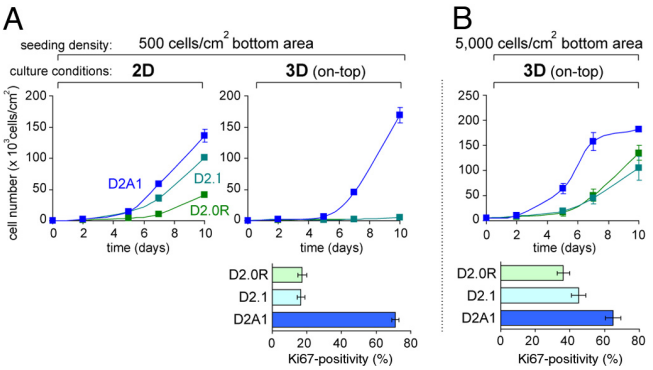

Fig. 2. Two-dimensional and 3-dimensional culture of nonmetastatic and metastatic D2 cells. (*A* and *B*) D2 cells were seeded at an initial density of either 500 cells/cm^2 bottom area (*A*) or 5,000 cells/cm^2 bottom area (*B*) and propagated under 2D or 3D on-top conditions. Cell numbers were determined at the indicated time points (*Top*). Cells cultured under 3D on-top conditions for 5 days were also stained for proliferation marker (Ki67), and the positivity of Ki67 staining within each cell population is plotted (*Bottom*).

try a modified version of the Matrigel-based 3D culture method. In particular, we cultured these various cells above a thin layer of Matrigel ("3D on-top"; Fig. S1*A*); under these conditions, the cells eventually invaded the Matrigel, reaching various depths within the Matrigel layer (Fig. S2).

As was the case with the previously used 3D-embedded culture method, we observed a sharp increase in the number of D2A1 cells and minimal increases in the numbers of D2.0R and D2.1 cells in these 3D on-top conditions (Fig. 2*A*); this difference in the rates of increase in cell numbers under 3D on-top conditions is consistent with a recent report by others (15). Under these conditions, the metastatic D2A1 cells exhibited a far higher positivity of the Ki67 proliferation marker than the nonmetastatic D2.0R and D2.1 cells cultured in parallel (Fig. 2*A* and Fig. S3*A*). In contrast, the extent of apoptosis was comparable among these 3 cell populations (Fig. S3*A*). Hence, the differing rates of increase in cell number among these various D2 cell populations under 3D culture conditions (Fig. 2*A*) was attributable to differing rates of cell-cycle progression rather than differences in rates of attrition by apoptosis.

To determine whether the initial seeding density affected the subsequent proliferation of cells, we also seeded the 3 different D2 cell populations in 3D on-top conditions at a 10-fold higher initial density (5,000 cells/cm^2 bottom area). Under these conditions, even the nonmetastatic D2.0R and D2.1 cells showed rapid increases in cell number during the ensuing 10 days (Fig. 2*B*). Thus, these cells exhibited higher Ki67 positivity than the same cell types seeded in 3D on-top conditions at the previously used sparse initial density (500 cells/cm^2 bottom area; Fig. 2 and Fig. S3). These results indicated that under high seeding densities, the control mechanisms that otherwise would preclude the nonmetastatic D2.0R and D2.1 cells from proliferating can be overridden, ostensibly because of cell–cell interactions or the altered interaction of cells with Matrigel. Indeed, when seeded at a density of 5,000 cells/cm^2 bottom area, even the D2.1 cells, which largely stayed as solitary cells within Matrigel for up to 10 days after being seeded at a low initial density (500 cells/cm^2; Fig. S3*A*), eventually aggregated and formed large clumps (Fig. S3*B*), within which individual cells are no longer surrounded on all sides by Matrigel. Thereafter, to observe maximal differences in vitro between the cell populations that do and do not proliferate effectively after extravasation in vivo, we used this 3D on-top method at a seeding density of 500 cells/cm^2 bottom area unless otherwise indicated.

As we continued to propagate the 3 different D2 cell populations in 3D culture for periods of up to 10 days, we noticed that a portion of these cells invaded through the Matrigel layer and began growing close to the bottom of the culture dish (data not shown). This invasion raised the possibility that the D2A1 cells proliferated more rapidly than the other 2 lines (Fig. 2*A*) simply because of their increased ability to invade through the Matrigel layer and ultimately to adhere to the substrate provided by the bottom of the culture dish. However, coating the dishes with poly(2-hydroxyethyl methacrylate) (polyHEMA), which inhibits the direct attachment of the cells to the plastic substrate, did not have significant effect on the number of D2A1 cells after 10 days of 3D culture (Fig. S4). Hence, the observed difference in the proliferation between the D2A1 cells and the other 2 lines after propagating them in 3D culture (Fig. 2*A*) appeared to derive from their superior ability to adapt to the microenvironmental conditions created by the Matrigel surrounding them.

We wished to gain insight into the underlying causes of the differing rates of cell-cycle progression in the various D2 cell populations propagated in 3D culture. Accordingly, we monitored changes in mRNA expression levels of genes encoding key cell-cycle regulators. We found that *p16^{Ink4a}*, *p19^{Arf}*, *p21^{Cip1}*, and *p27^{Kip1}*, all of which yield proteins having an inhibitory effect on cell-cycle progression, were up-regulated in D2.0R and D2.1 cells under 3D but not under 2D conditions (Fig. S5*A*). Moreover, proliferation of the slowly growing D2.0R and D2.1 cells in 3D culture was partially restored by shRNA-mediated, simultaneous knockdown of the expression of p16^{Ink4a} and p19^{Arf} (Fig. S5*B*). Hence, the minimal increases in the numbers of D2.0R and D2.1 cells propagated under 3D conditions were attributable to inhibition of cell-cycle progression, which could be explained, at least in part, by the up-regulation of the *p16^{Ink4a}* and *p19^{Arf}* mRNAs and the cell-cycle inhibitory function of the corresponding protein products.

To determine whether the 3D on-top culture condition also yields differing rates of proliferation in other sets of related cancer cell lines with distinct metastatic potentials, we studied the B16F1 and B16F10 mouse melanoma cell lines, which exhibit low and high efficiencies of generating lung metastases, respectively. When propagated under 3D on-top conditions, the highly metastatic B16F10 cells proliferated more rapidly than the weakly metastatic B16F1 cells, resulting in a 2.4-fold difference in cell number after 10 days of culture, whereas their proliferation rates under 2D culture conditions were comparable (Fig. S6). Taken together, these various results showed a strong correlation between the proliferative capacity of cells in 3D culture and their metastasis-forming ability.

Signals from Cell-Matrix Adhesions Regulate the Proliferation of Cancer Cells Scattered Within the ECM. The observations described above encouraged us to determine the biochemical mechanism(s) responsible for the differing abilities of the various D2 cell populations to proliferate in the 3D culture model. Microscopic observations of these cell populations revealed striking morphological differences between them under 3D on-top culture conditions. Three-dimensionally cultured D2.0R cells typically displayed a round morphology and formed small clumps (Fig. 3*A* and Fig. S3*A*). A large part of D2.1 cells exhibited a narrow, elongated morphology (Fig. 3 *A* and Fig. S3*A*). The metastatic D2A1 cells were also elongated, but tended to have protrusive extensions and their cytoplasm was wider than that of D2.1 cells (Fig. 3 *A* and Fig. S3*A*). These differences in morphology suggested underlying differences in the organization of the respective cytoskeletons. Indeed, we saw the abundant formation of actin stress fibers in all of the 3 cell types under 2D conditions of culture, whereas under 3D conditions, only the metastasis-competent D2A1 cells exhibited these fibers (Fig. S7*A*).

The formation of these stress fibers is known to be regulated by integrin-mediated adhesions to the ECM (16). Accordingly, we used immunofluorescence to survey the localization of adhesion plaque proteins, specifically paxillin, vinculin, and talin, whose patterns of localization reflect the degree of maturation of integrin-mediated adhesions (16). In fact, the localization of these proteins

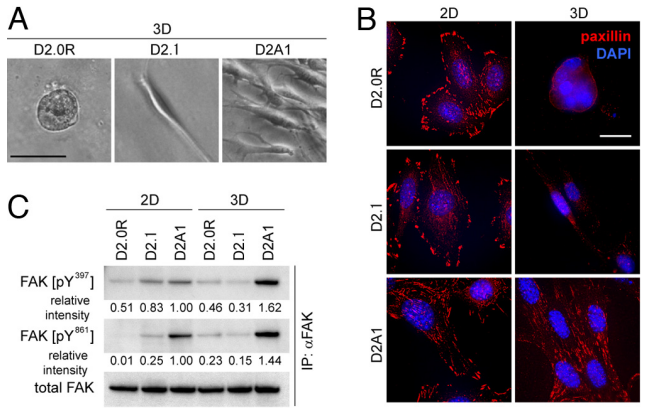

Fig. 3. Cell-matrix adhesions of 2D- and 3D-cultured D2 cells. (*A*) D2 cells were propagated under 3D on-top culture conditions, and the typical morphologies of cells after 10 days of culture are presented. (Scale bar, 50 μm.) (*B*) D2 cells cultured under 2D or 3D conditions for 5 days were stained for paxillin (red), and the nuclei were stained with DAPI (blue). (Scale bar, 20 μm.) (*C*) To assess the levels of FAK phosphorylation, cell lysates were immunoprecipitated with anti-total FAK antibody, and the precipitates were analyzed by immunoblotting. Values are the band intensities relative to that of the corresponding band of the sample from 2D-cultured D2A1 cells.

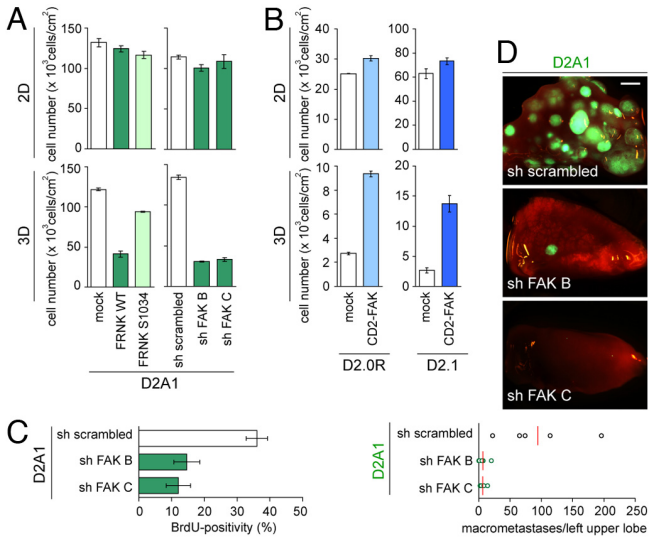

Fig. 4. The effects of manipulating FAK signaling on the in vitro and in vivo proliferation of D2 cells. (*A*) The effects of wild-type or mutant FRNK (FRNK WT and FRNK S1034, respectively) expression and FAK knockdown on the proliferation of D2A1 cells under 2D and 3D conditions of culture were analyzed. Proliferation of 3D-cultured D2A1 cells was impaired by expressing FRNK WT, but not by expressing FRNK S1034, in which dominant-negative effect is abrogated (*Left*). In the *Right* graphs, the effects of 2 different shRNA constructs targeting FAK expression (sh FAK B and C) and the effect of an shRNA control (sh scrambled) are presented (Table S1). Here, and in *B*, cell numbers were determined after 10 days of culture. (*B*) The effects of CD2-FAK expression on the proliferation of D2.0R and D2.1 cells under 2D and 3D conditions of culture were analyzed. (*C*) The effect of FAK knockdown on the BrdU incorporation by D2A1 cells after extravasation in the lungs in vivo was analyzed as in Fig. 1*C*. (*D*) Lungs were harvested at 24 days after the tail-vein injection of GFP-labeled D2A1 cells expressing an shRNA control (sh scrambled) or GFP-labeled FAK knockdown D2A1 cells (sh FAK B or C). Shown are the representative images of the left upper lobe of the lungs (*Top*). (Scale bar, 1 mm.) The numbers of macroscopic metastases observed on the surface of the left upper lobe are plotted (*Bottom*). The red bar indicates the mean value in each sample group. Values are means ± SD ($n = 3$) (*A* and *B*) or means ± SEM ($n = 4$) (*C*).

to plaques with an oval-like or elongated morphology, which is typical of the mature form of adhesion plaques, was clearly observed in all 3 cell populations cultured under 2D conditions (Fig. 3*B* and Fig. S7 *B* and *C*). Under 3D on-top culture conditions, however, only the D2A1 cells developed abundant adhesion plaques of elongated morphology (Fig. 3*B* and Fig. S7 *B* and *C*). To summarize, the D2A1 cells, which proliferated well under 3D conditions, exhibited extensive actin stress fibers and mature forms of integrin-associated adhesion plaques under both 2D and 3D conditions of culture, whereas the D2.0R and D2.1 cells, which failed to proliferate efficiently under 3D conditions, were only able to assemble dense actin stress fibers and mature adhesion plaques under 2D conditions of culture.

The correlation between the formations of mature adhesion plaques and proliferation suggested a causal relationship between these processes. In this regard, integrin-mediated adhesions have been shown to trigger the release of a variety of intracellular signals, which together represent the "outside-in" signaling by integrins (17). This evidence suggested that the differing abilities to form integrin-mediated adhesions among the various D2 cell populations under 3D conditions (Fig. 3*B* and Fig. S7 *B* and *C*) might lead, in turn, to differential activation of the downstream signaling events within these cells, and such signaling might ultimately determine the differing abilities to proliferate under these conditions (Fig. 2*A*).

Among the signals arising from the formation of cell-matrix adhesions, FAK is thought to play a central role (18). Thus, FAK has been shown to play an essential role in promoting cell-cycle progression in a variety of cell types (19). Recruitment of FAK by ECM-ligated integrins induces its autophosphorylation at tyrosine 397 (Y397). Y397-phosphorylated FAK in turn binds to another tyrosine kinase, Src, which phosphorylates FAK at tyrosine 861 (Y861). This Y861 phosphorylation then facilitates the recruitment of p130Cas to FAK, which leads ultimately to the activation of multiple signaling proteins, including the Ras and Rac small GTPases (18).

For these reasons, we analyzed FAK phosphorylation at Y397 and Y861 in 2D- and 3D-cultured D2 cells and discovered strong differences in the levels of phosphorylation among the different cell populations, particularly under 3D culture conditions (Fig. 3 *C* and Fig. S7*D*). Thus, 3D-cultured metastasis-competent D2A1 cells exhibited 3.5- to 5.2-fold and 6.3- to 9.6-fold higher levels of phosphorylation at FAK Y397 and Y861, respectively, compared with the other 2 cell lines cultured in parallel (Fig. 3*C*). This result revealed a strong correlation between proliferative ability and FAK Y397 and Y861 phosphorylation in 3D-cultured D2 cells.

Given this correlation, we speculated that the functional activation of FAK might represent a rate-limiting determinant of proliferative ability in 3D culture. Consequently, we modulated its activity through the ectopic expression of FAK-related nonkinase (FRNK), a naturally existing, dominant-negative variant of FAK. Indeed, ectopic FRNK expression in D2A1 cells inhibited their proliferation under 3D but not under 2D conditions of culture (Fig. 4*A*). Similarly, knocking down the expression of FAK using shRNA also resulted in impaired proliferation of 3D-cultured D2A1 cells (Fig. 4*A*). Conversely, ectopic expression in D2.0R and D2.1 cells of a CD2-FAK fusion protein, which exhibits constitutive kinase activity (20), partially rescued their proliferation defects under 3D culture conditions (Fig. 4*B*). These results confirmed the central role of integrin-activated FAK signaling in regulating the proliferation of the various D2 cell types under 3D conditions of culture.

We proceeded to determine the role of FAK signaling in the process of metastatic colony formation in vivo. Twelve hours after coinjecting equal numbers of tdTomato-labeled control D2A1 cells and GFP-labeled FAK-knockdown D2A1 cells through the tail vein, we found a 2.9- to 3.2-fold greater number of control cells remaining in the lungs after perfusion with FluoSpheres than those of corresponding FAK-knockdown cells (Fig. S8). At 48 h after injection, however, we detected comparable numbers of perfusion-resistant control and FAK-knockdown D2A1 cells in the lungs (Fig.

S8), which collectively indicated that knocking down the expression of FAK delays the extravasation of D2A1 cells into the lung parenchyma, but does not affect the long-term extravasation efficiency. In contrast to this, the proliferation of the extravasated cells monitored at 7 days after injection, and the formation of metastatic colonies examined at 24 days after injection, were both significantly impaired by knocking down FAK expression (Fig. 4 *C* and *D*). These results demonstrated that FAK signaling controls the metastatic colony-forming ability of D2A1 cells in the lungs largely by regulating their postextravasation proliferation.

Attachment to the ECM via β_1-Containing Integrins Is Essential for FAK Activation and Cell Proliferation. We attempted to address the mechanism regulating FAK phosphorylation, which contributed significantly to the differing rates of proliferation observed in the various D2 cell populations under 3D on-top culture conditions. Integrins govern the activity of FAK, and there are 24 different heterodimeric pairs of these proteins functioning in various mammalian cell types. With the exception of those expressed specifically in hematopoietic cells, these integrin pairs are categorized in 3 groups: β_1-containing integrins, α_v-containing integrins ($\alpha_v\beta_3$, $\alpha_v\beta_5$, $\alpha_v\beta_6$, and $\alpha_v\beta_8$), and $\alpha_6\beta_4$-integrin (17); among these, the β_1-containing and α_v-containing ones play central roles in recruiting and activating FAK (16). To determine which particular pair(s) of integrin contribute(s) to FAK activation and, in turn, to cell proliferation under 3D conditions, we used shRNAs to knockdown the expression of the constituent subunits of several integrin pairs of special interest and examined resulting effects on the proliferation of D2A1 cells under either 2D or 3D conditions of culture.

Most notably, knocking down integrin β_1 expression almost completely blocked the proliferation of D2A1 cells under 3D but not under 2D conditions (Fig. 5*A*). Moreover, knocking down the expression of either integrin α_3 or integrin α_5, both of which are paired exclusively with integrin β_1, partially impaired D2A1 cell proliferation, once again under 3D but not under 2D conditions (Fig. 5*A*). In contrast, knocking down the expression of either integrin α_v or integrin α_6 did not show any inhibitory effect on the proliferation of 3D-cultured D2A1 cells (Fig. 5*A*). Hence, the proliferation of D2A1 cells cultured under these Matrigel-based 3D on-top conditions depended on the expression of β_1-containing integrins, but not on either α_v-containing integrins or $\alpha_6\beta_4$-integrin.

We examined whether the β_1-containing integrins exhibited superior ability to recruit and thereby activate FAK in 3D-cultured D2A1 cells compared with α_v-containing integrins, the other group of integrins playing major roles in regulating FAK function, by using immunofluorescence. We observed that under 3D conditions, the staining of FAK in D2A1 cells overlapped well with those of integrin β_1 and integrin α_5, a major dimerization partner of integrin β_1 (Fig. 5*B*). In contrast, there was almost no overlap between the staining of FAK and that of integrin α_v in these cells (Fig. 5*B*). Moreover, knocking down the expression of integrin β_1 in 3D-cultured D2A1 cells resulted in a >4-fold reduction in the levels of FAK phosphorylation at residues Y397 and Y861 (Fig. 5*C*).

These results collectively supported the notion that attachment to the ECM via β_1-containing integrins plays an essential role in causing FAK phosphorylation in 3D-cultured D2A1 cells and ultimately enables the efficient proliferation of these cells. Consistent with this notion, under 3D culture conditions of culture, knocking down the expression of either integrin β_1 or FAK in D2A1 cells resulted in the up-regulation of mRNAs encoding the $p16^{Ink4a}$, $p19^{Arf}$, $p21^{Cip1}$, and $p27^{Kip1}$ cell-cycle regulators (Fig. S9); as described earlier, elevated expression of these mRNAs was correlated with proliferation arrest in the 3D-cultured, nonmetastatic D2.0R and D2.1 cells (Fig. S5*A*). Consistent with this notion, in vivo proliferation of D2A1 cells after extravasation into the lung parenchyma was inhibited by knocking down the expression of integrin β_1 (Fig. 5*D*), similar to the effect of FAK knockdown (Fig. 4*C*). This provided further evidence that the integrin β_1-FAK signaling axis

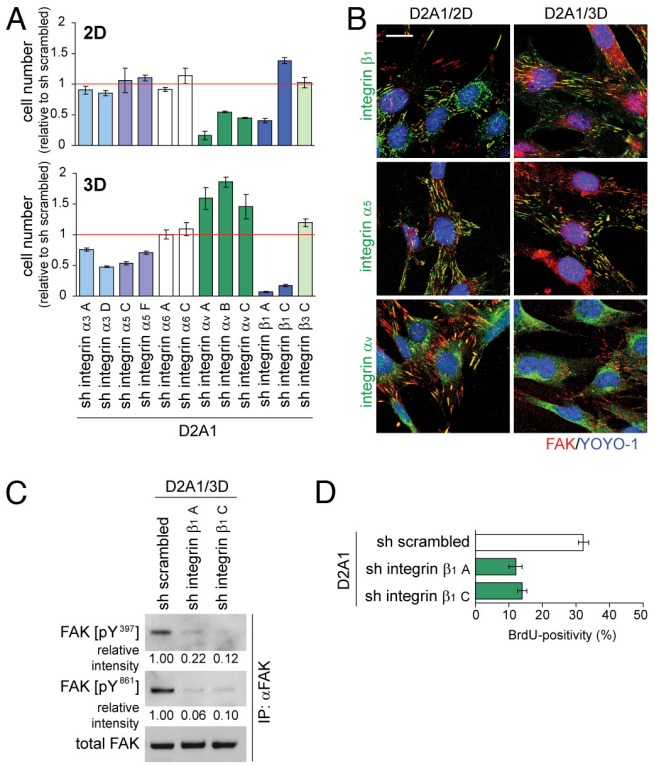

Fig. 5. Recruitment and activation of FAK by β_1-containing integrins in 3D-cultured D2A1 cells. (*A*) The effects of integrin subunit knockdown on the proliferation of D2A1 cells under 2D and 3D conditions of culture were analyzed. Cells were cultured for 10 days. The capital letter at the end of each shRNA label is added for distinguishing different shRNA constructs for the same target, and multiple different constructs were tested for targeting each of integrin α_3, α_5, α_6, α_v, and β_1 expression, whereas a single shRNA construct was tested for targeting the expression of integrin β_3 (sh integrin β_3 C) (Table S1 and Table S2). Cell numbers relative to that of D2A1 cells expressing an shRNA control (sh scrambled) are plotted. Values are means ± SD ($n = 3$). (*B*) Colocalization between FAK (red) and integrin β_1, integrin α_5, or integrin α_v (green) in D2A1 cells under 2D or 3D culture conditions (Matrigel, on-top) was analyzed by immunofluorescence. Cell nuclei were stained with YOYO-1 (blue). (Scale bar, 20 μm.) (*C*) The effects of integrin β_1 knockdown on the levels of FAK phosphorylation at Y397 and Y861 in 3D-cultured D2A1 cells were analyzed as in Fig. 3*C*. Two different shRNA constructs targeting the expression of integrin β_1 were tested (sh integrin β_1 A and C). Values are the band intensities relative to that of the corresponding bands of the sample from D2A1 cells expressing an shRNA control (sh scrambled). (*D*) The effect of integrin β_1 knockdown on the BrdU incorporation by D2A1 cells after extravasation in the lungs in vivo was analyzed as in Fig. 1*C*. Values are means ± SEM ($n = 4$).

is essential for the postextravasation proliferation of D2A1 cells in the lungs.

Discussion

Only rare disseminated cancer cells are able to found metastatic colonies, usually only after a prolonged period. This inefficient colony formation has been ascribed to a number of factors, among them the complex adaptations that cancer cells must make to thrive in the foreign tissue microenvironments in which they find themselves after dissemination. In the present study, we have exploited an in vitro, 3D culture model to examine how disseminated cancer cells cope with their initially low density within the parenchyma of such tissues and with their need to associate productively with components of the ECM, which represent key functional elements of these microenvironments (Fig. S1*A*). Whereas this 3D culture model does not faithfully recapitulate all aspects of the in vivo microenvironment, it

sufficed to reveal a strong difference in proliferative behavior between cancer cells that can or cannot colonize the lung tissues in vivo (Fig. 2*A*, Fig. S1, Fig. S3*A*, and Fig. S6).

As we found, under 3D on-top conditions of culture, the D2.0R and D2.1 cells, which can extravasate but fail to colonize in the lungs, showed patterns of adhesion to the ECM that were very different from that of the related, highly metastatic D2A1 cells (Fig. 3*B* and Fig. S7 *B* and *C*): only the D2A1 cells but not D2.0R and D2.1 cells developed abundant adhesion plaques of elongated morphology, these being typical of the mature form of adhesion plaques. Thus, earlier studies of 2D-cultured fibroblasts had demonstrated that matrix adhesion plaques initially appear as small dots at the periphery of cells, which subsequently mature both morphologically and functionally: This maturation involves conversion of dot-like plaques into oval-like or elongated forms and an increase in the overall levels of FAK phosphorylation (16).

Consistent with these previous observations, the D2A1 cells exhibited higher levels of FAK phosphorylation at both the Y397 and Y861 residues under 3D conditions than did the D2.0R and D2.1 cells cultured in parallel (Fig. 3*C*); this ultimately contributed to the rapid proliferation of D2A1 cells under these conditions (Fig. 2*A*). Because the proliferation of cells extravasated in the lungs in vivo was also highly dependent on FAK signaling (Fig. 4*C*), we conclude that the postextravasation proliferation of cancer cells disseminated throughout the lung tissue is governed by the ability of these cells to successfully develop mature adhesion plaques to the ECM and thereby to efficiently activate FAK signaling.

Previous reports have shown that inhibiting the kinase activity of FAK or knocking down the expression of FAK in various other lines of breast cancer cells also results in reduced formation of metastatic colonies in the lungs (21–23), because of either impairment of invasive migration or reduced efficiency of extravasation. Taken together with the present results, it now appears that FAK signaling exerts regulatory effects on multiple different steps of the invasion–metastasis cascade.

We have also found the essential roles of β_1-containing integrins in enabling efficient proliferation of D2A1 cells both under 3D culture conditions in vitro and after disseminating into the lung parenchyma in vivo (Fig. 5 *A* and *D*). These results are indeed consistent with the reported function of β_1-containing integrins (17); these integrins are involved in the adhesion to type I and type III collagen, main constituents of the lung parenchyma (24), and moreover, they also bind to laminin and type IV collagen, major components of Matrigel, which is used as substrate for the 3D culture described here.

Under in vitro 3D culture conditions in D2A1 cells, β_1-containing integrins played essential roles in enabling efficient FAK phosphorylation (Fig. 5 *B* and *C*), which explains how these integrins contribute to the proliferation of D2A1 cells under these conditions. Shortly after introducing them into 3D culture, the nonmetastatic D2.0R and D2.1 cells exhibited levels of integrin β_1 and FAK expression comparable to those found in the metastatic D2A1 cells (T.S. and R.A.W., unpublished observations). However, these nonmetastatic cells showed lower levels of FAK phosphorylation (Fig. 3*C*), which appears to be the result, in turn, of the mechanisms regulating the formation of cell-matrix adhesions via β_1-containing integrins. Studying the details of such regulation will surely provide one important key to understanding how cancer cells adapt to the foreign tissue microenvironment that they initially encounter after metastatic dissemination and extravasation. This process, in turn, appears to strongly influence the efficiency of eventual colonization by these disseminated cancer cells.

Methods

Cell Culture. For the 3D on-top culture, 12-well culture plates were coated with 160 μL/well of Matrigel (BD Biosciences) and incubated at 37°C for 30 min, which allowed the Matrigel to solidify. Subsequently, cells (500 cells/cm^2 bottom area; 2,000 cells for 12-well plate, unless otherwise indicated) were resuspended as single cells in 1 mL of 2D/3D culture medium (DME/F12 medium supplemented with 2% horse serum, 0.5 μg/mL hydrocortisone, 50 ng/mL cholera toxin, 10 μg/mL insulin, 100 U/mL penicillin and 100 μg/mL streptomycin) containing 2% Matrigel, and added on top of Matrigel. For the 2D culture in 12-well culture plates, 2,000 cells were resuspended in 1 mL of 2D/3D culture medium and directly plated in the well. Medium was changed every 4 days.

Animal Procedures. Two- to four-month-old male BALB/c mice were used for tail-vein injections. One hundred microliters of cancer cells resuspended in PBS were injected through the tail vein. The number of cells injected per mouse in each experiment is the following: 5×10^5 for each of GFP-labeled and tdTomato-labeled cells in Fig. 1*A*, 1×10^6 for each of GFP-labeled and tdTomato-labeled cells in Fig. 1*B* and Fig. S8, 1×10^6 cells in Figs. 1*C*, 4*C*, and 5*D* and 5×10^5 cells in Fig. 4*D*. For the perfusion of lung microvasculature, mice were anesthetized by the i.p. injection of 100 mg/kg ketamine and 10 mg/kg xylene, and then the chest was opened and an incision was made on the wall of the left ventricle. Subsequently, 6 mL of PBS, followed by 2 mL of FluoSpheres (Invitrogen; 0.2 μm, europium luminescence), diluted 1:4 with PBS, was injected into the right ventricle.

Statistical Analyses. Statistical analyses were performed by Student's *t* test.

ACKNOWLEDGMENTS. We thank R. J. Lee, F. Reinhardt, T. Chavarria, E. Batchelder, and E. Vasile for technical assistance; S. Godar, S. S. McAllister, M. P. Saelzler, K. J. Kah for discussions; F. R. Miller, R. Y. Tsien, D. D. Schlaepfer, I. Ben-Porath, D. Trono, S. M. Frisch, and K. Vuori for reagents. T.S. is a recipient of a long-term fellowship from the Human Frontier Science Program and postdoctoral fellowship from the Japan Society for the Promotion of Science. R.A.W. is an American Cancer Society research professor and a Daniel K. Ludwig Foundation cancer research professor. This work was funded by grants from the Ludwig Center for Molecular Oncology at MIT (R.A.W.), the Breast Cancer Research Foundation (R.A.W.); NIH U54 CA12515 (R.A.W.).

1. Fidler IJ (2003) The pathogenesis of cancer metastasis: The 'seed and soil' hypothesis revisited. *Nat Rev Cancer* 3:453–458.
2. Braun S, et al. (2005) A pooled analysis of bone marrow micrometastasis in breast cancer. *N Engl J Med* 353:793–802.
3. Aguirre-Ghiso JA (2007) Models, mechanisms and clinical evidence for cancer dormancy. *Nat Rev Cancer* 7:834–846.
4. Mareel MM, De Baetselier P, Roy MV (1991) *Mechanism of Invasion and Metastasis* (CRC press, Boca Raton), 1st Ed, p 584.
5. Mehlen P, Puisieux A (2006) Metastasis: A question of life or death. *Nat Rev Cancer* 6:449–458.
6. Naumov GN, et al. (2002) Persistence of solitary mammary carcinoma cells in a secondary site: A possible contributor to dormancy. *Cancer Res* 62:2162–2168.
7. Schmidt-Kittler O, et al. (2003) From latent disseminated cells to overt metastasis: Genetic analysis of systemic breast cancer progression. *Proc Natl Acad Sci USA* 100:7737–7742.
8. Rak JW, McEachern D, Miller FR (1992) Sequential alteration of peanut agglutinin binding-glycoprotein expression during progression of murine mammary neoplasia. *Br J Cancer* 65:641–648.
9. Morris VL, et al. (1994) Mammary carcinoma cell lines of high and low metastatic potential differ not in extravasation but in subsequent migration and growth. *Clin Exp Metastasis* 12:357–367.
10. Shaner NC, et al. (2004) Improved monomeric red, orange and yellow fluorescent proteins derived from Discosoma sp. red fluorescent protein. *Nat Biotechnol* 22:1567–1572.
11. Springer ML, Ip TK, Blau HM (2000) Angiogenesis monitored by perfusion with a space-filling microbead suspension. *Mol Ther* 1:82–87.
12. Poste G, et al. (1982) Evolution of tumor cell heterogeneity during progressive growth of individual lung metastases. *Proc Natl Acad Sci USA* 79:6574–6578.
13. Nelson CM, Bissell MJ (2006) Of extracellular matrix, scaffolds, and signaling: Tissue architecture regulates development, homeostasis, and cancer. *Annu Rev Cell Dev Biol* 22:287–309.
14. Debnath J, Brugge JS (2005) Modelling glandular epithelial cancers in three-dimensional cultures. *Nat Rev Cancer* 5:675–688.
15. Barkan D, et al. (2008) Inhibition of metastatic outgrowth from single dormant tumor cells by targeting the cytoskeleton. *Cancer Res* 68:6241–6250.
16. Geiger B, Bershadsky A, Pankov R, Yamada KM (2001) Transmembrane crosstalk between the extracellular matrix–cytoskeleton crosstalk. *Nat Rev Mol Cell Biol* 2:793–805.
17. Hynes RO (2002) Integrins: Bidirectional, allosteric signaling machines. *Cell* 110:673–687.
18. Tilghman RW, Parsons JT (2008) Focal adhesion kinase as a regulator of cell tension in the progression of cancer. *Semin Cancer Biol* 18:45–52.
19. Assoian RK, Klein EA (2008) Growth control by intracellular tension and extracellular stiffness. *Trends Cell Biol* 18:347–352.
20. Chan PY, Kanner SB, Whitney G, Aruffo A (1994) A transmembrane-anchored chimeric focal adhesion kinase is constitutively activated and phosphorylated at tyrosine residues identical to pp125FAK. *J Biol Chem* 269:20567–20574.
21. Benlimame N, et al. (2005) FAK signaling is critical for ErbB-2/ErbB-3 receptor cooperation for oncogenic transformation and invasion. *J Cell Biol* 171:505–516.
22. Lahlou H, et al. (2007) Mammary epithelial-specific disruption of the focal adhesion kinase blocks mammary tumor progression. *Proc Natl Acad Sci USA* 104:20302–20307.
23. Pylayeva Y, et al. (2009) Ras- and PI3K-dependent breast tumorigenesis in mice and humans requires focal adhesion kinase signaling. *J Clin Invest* 119:252–266.
24. Suki B, Ito S, Stamenovic D, Lutchen KR, Ingenito EP (2005) Biomechanics of the lung parenchyma: Critical roles of collagen and mechanical forces. *J Appl Physiol* 98:1892–1899.